Supporting Information

Nanowire Forest of Pnictogen-Chalcogenide alloys for Thermoelectricity

Dhruv Singhal,[†,‡,¶] Jessy Paterson,[‡,¶] Meriam Ben-Khedim,[‡,¶,§] Dimitri Tainoff,[‡,¶] Laurent Cagnon,[‡,¶] Jacques Richard,[‡,¶] Emigdio Chavez-Angel,[‖] Juliana Jaramillo-Fernandez,[‖] Clivia M. Sotomayor-Torres,[‖,⊥] David Lacroix,[#] Daniel Bourgault,[‡,¶] Denis Buttard,[†,¶] and Olivier Bourgeois[*,‡,¶]

†*Univ. Grenoble Alpes, CEA, INAC-Pheliqs, F-38000 Grenoble, France*

‡*Institut NÉEL, CNRS, 25 avenue des Martyrs, F-38042 Grenoble, France*

¶*Univ. Grenoble Alpes, Grenoble, France*

§*Technology R&D, STMicroelectronics, 13106 Rousset, France*

‖*Catalan Institute of Nanoscience and Nanotechnology (ICN2), CSIC and BIST, Campus UAB, Bellaterra 08193 Barcelona, Spain*

⊥*ICREA, Passeig Lluís Companys 23, 08100 Barcelona, Spain*

#*Université de Lorraine, CNRS, LEMTA, Nancy, F-54000 FRANCE*

E-mail: olivier.bourgeois@neel.cnrs.fr

Fabrication of nanowire ensemble

Anodisation of aluminium was performed at 40 V in the electrolyte of oxalic acid (0.5 M), which was regulated at 16°C, via two-step anodisation[S1] process in order to have homogeneous pore diameter. This process resulted in the pore diameter of 69±4 nm and the

final thickness of 60 μm (which is only dependent on the initial thickness of aluminium used for anodisation). Electrodeposition was performed after metallising the back side of the nanoporous alumina with Ti (10 nm thick) buffer layer followed by Au (200 nm thick) layer. The electrolytes used were based on the previous studies of Bu *et al.*[S2] and Del Frari *et al.*[S3] on $Bi_2Te_{3-y}Se_y$ nanowires and $Bi_{2-x}Sb_xTe_3$ thin films respectively, with a slight modification to achieve the ideal stoichiometry in these alloys (i.e. $Bi_2Te_{2.7}Se_{0.3}$ for n-type and $Bi_{0.5}Sb_{1.5}Te_3$ for p-type) for room temperature applications.[S4,S5]

The electrolytes are composed of $HClO_4$ 1 M solution containing 10 mM Bi_2O_3, 10.3 mM TeO_2 and 1.1 mM SeO_2 for n-type ($Bi_2Te_{3-y}Se_y$), and 2 mM Bi_2O_3, 12 mM TeO_2 and 12 mM Sb_2O_3 in 0.4 M tartaric acid for p-type ($Bi_{2-x}Sb_xTe_3$). For the pulse electrodeposition of n-type nanowires, the potentials applied were 0 V and -0.2 V, while for the p-type, potentials were -0.15 V and -0.3 V. More detailed information about the pulse durations and electrodeposition setup is described in the reference.[S6] The embedded nanowire film was annealed at 523 K under Ar/H_2 for four hours to improve the crystalline structure. Figure S1 shows high-resolution TEM micrographs of the nanowires.

The nanowires were overgrown out of the nanoporous alumina templates through pulse electrodeposition. The kinetics of growth is not homogeneous in each and every pore of the template. In order to achieve a smooth surface with same height of nanowires and high-pore filling ratio, Chemical Mechanical Polishing (CMP) is used for planarization.

The nanowires were then characterised for the composition and crystal structure. AAO was chemically etched to acquire free standing nanowires. The nanowires were then dispersed in IPA, which was later put on the TEM grids by drop casting. The compositional analysis was carried out on multiple nanowires simultaneously by energy-dispersive X-ray spectroscopy (EDX) in scanning electron microscope (SEM) in cross-section. In figure S2b, it can be seen that the stoichiometry of the alloy is constant throughout the length of nanowires. Similar measurement were carried out to determine the stoichiometry of the other three ternary alloys as well.

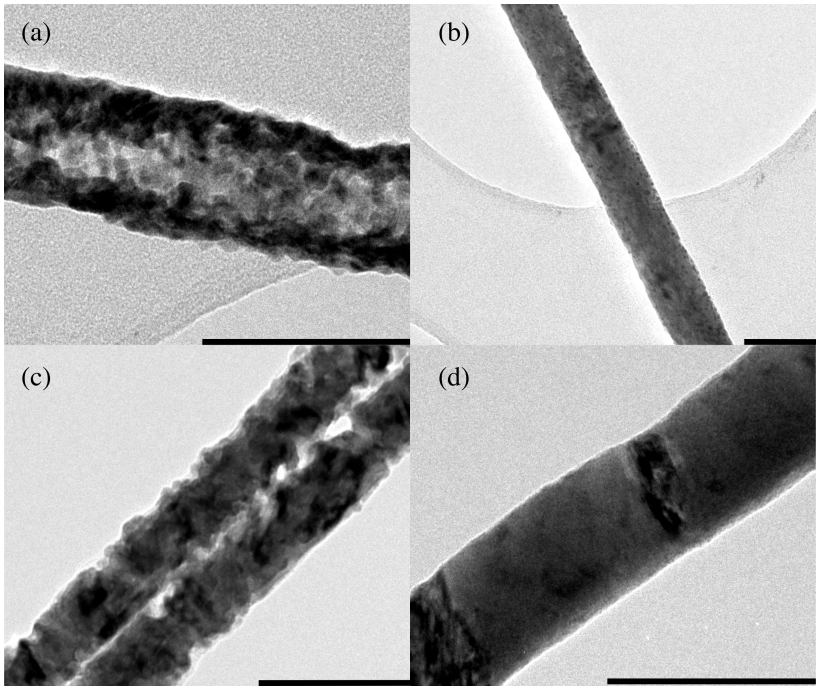

Figure S1: Transmission electron micrographs of single nanowires performed after etching AAO. (a) $Bi_{1.45}Te_{2.85}Se_{0.7}$ nanowires electro-deposited at -0.2 V, (b) $Bi_{1.55}Te_{2.9}Se_{0.55}$ nanowires deposited at 0 V, (c) $Bi_{0.4}Sb_{1.43}Te_{3.17}$ nanowires deposited at -0.15 V and, (d) $Bi_{0.6}Sb_{1.85}Te_{2.55}$ nanowire deposited at -0.3 V. *Scale* on the images is 100 nm. (a) and (c) are comparatively rougher than (b) and (d).

Determination of thermal conductivity

The 3ω method is a well-established and precise measurement technique for determining the thermal conductivity of thin films and bulk materials.[S7–S17] This ac thermal conductivity measurement technique is less sensitive to the errors arising from the black-body radiation

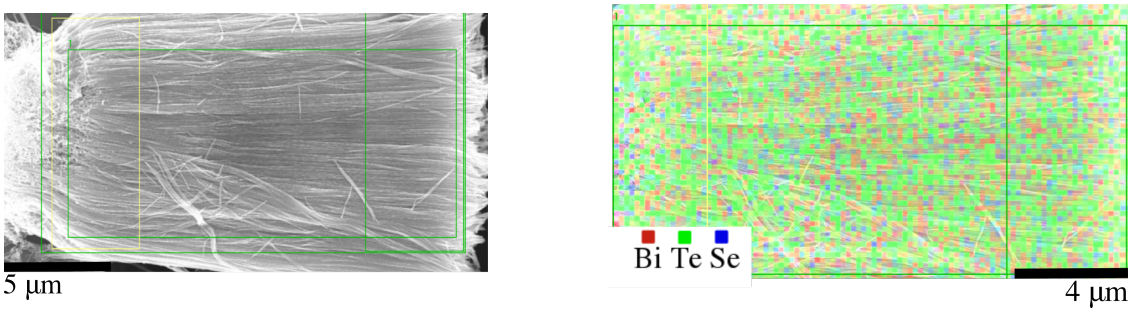

(a) (b)

Figure S2: Structural analysis of $Bi_{1.45}Te_{2.85}Se_{0.7}$ nanowires by (a) and (b) energy-dispersive X-ray spectroscopy in scanning electron microscope.

and these errors are scaled with the characteristic length of experimental geometry.[S7] In this method, a metallic strip (platinum) is deposited on top of the sample after isolating it electrically through an thin insulating layer (Al_2O_3). This metallic strip has a four-point probe geometry using a radial flow of heat from a single element, which acts as both, heater and thermometer (commonly referred to as transducer).

An applied alternating current with an angular frequency of ω causes temperature oscillations at 2ω due to Joule heating. The magnitude and phase of the oscillations depend on the vicinity of the transducer. The electrical resistance of the transducer is modulated at 2ω coupled through the temperature coefficient of the resistivity ($\alpha = \frac{1}{R}\frac{\partial R}{\partial T}$). The resulting third-harmonics of the voltage component contains the information of thermal properties of the underlying layers, which gives information of the thermal conductivity precisely down to thin films of several nanometers.[S7–S9] However, the ratio of amplitudes of $V_{3\omega}$ to $V_{1\omega}$ is small (normally, smaller than 10^{-3}), which requires the development of an active electronic circuit. In order to achieve a high signal-to-noise ratio, it is imperative to cancel out the large 1ω signal by using a cancellation step either through nullifying bridge[S18–S20] or by subtraction with multiplying digital-to-analog converter.[S9]

Usually, an approximate analytical expression is employed to determine the thermal conductivity k_0 which is based on slope of the real part of 3ω voltage expressed as a function of logarithmic electrical frequency.[S8,S9] However, there are limitations on the applicability of slope method which restricts the determination of thermal characterisations only for simple architectures. In this case, a 2D heat conduction thermal model given by Borca-Tasciuc et al.[S11] was used for the calculation of temperature rise in the general case of multilayer film-on-semi-infinite substrates. The complex temperature rise in the transducer which is dissipating a power P/l ($\mathrm{W.m^{-1}}$) (the peak electrical power per unit length) is given by:[S11]

$$\Delta T = \frac{-P}{\pi l \kappa_{y_1}} \int_0^\infty \frac{1}{A_1 B_1} \frac{\sin^2(b\lambda)}{b^2\lambda^2} d\lambda \tag{S1}$$

where,

$$A_{i-1} = \frac{A_i \dfrac{\kappa_{y_i} B_i}{\kappa_{y_{i-1}} B_{i-1}} - \tanh(\phi_{i-1})}{1 - A_i \dfrac{\kappa_{y_i} B_i}{\kappa_{y_{i-1}} B_{i-1}} \tanh(\phi_{i-1})} \ , \quad i = 2...n \tag{S2}$$

$$B_i = \left(\kappa_{xy_i} \lambda^2 + \frac{j\ 2\omega}{\gamma_{y_i}} \right)^{\frac{1}{2}} \tag{S3}$$

$$\phi_i = B_i d_i \qquad \kappa_{xy} = \frac{\kappa_x}{\kappa_y} \tag{S4}$$

where, n refers to the total number of layers including the substrate with subscript i for the i^{th} layer from the top, subscript x and y correspond respectively to the direction parallel and perpendicular to the transducer and to the film/substrate, b is the heater half width, κ is the thermal conductivity, κ_{xy} is the ratio of in-plane to the cross-plane thermal conductivity, d is the layer thickness and, γ is the thermal diffusivity. For the substrate layer, $i = n$ and for substrates with finite thickness, the value of A_n depends on the boundary condition at the bottom of the substrate. For adiabatic boundary conditions $A_n = -\tanh(B_n d_n)$ and for isothermal conditions, $A_n = -1/\tanh(B_n d_n)$. $A_n = -1$ if the substrate is semi-infinite.

Considering the impact of heater's thickness (d_h), heat capacity c_h, and thermal boundary resistance (R_{th}) between the heater and film in contact with the heater to the complex temperature rise of the heater, it is modified as:[S11]

$$T_h = \frac{\Delta T + R_{th} p/2bl}{1 + (\rho c)_h d_h i 2\omega (R_{th} + \Delta T 2bl/p)} \tag{S5}$$

where ΔT is the average complex temperature rise determined from Eq. S1 under the same heating power. This analytical solution has been applied to determine thermal conductivity of the array of nanowires embedded in anodic aluminium oxide films.[S21]

The fabricated forest of nanowires embedded in amorphous nanoporous alumina templates have anisotropic thermophysical properties arising intrinsically from the structure. Thus, the calculation of anisotropy factor holds prime importance in determining the ther-

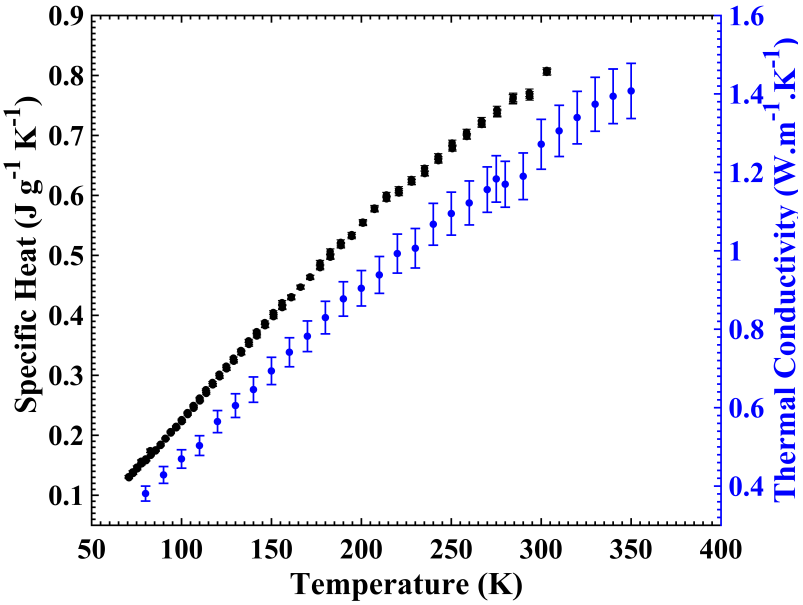

Figure S3: The variation of specific heat and thermal conductivity of empty nanoporous alumina templates with temperature are presented. The specific heat measurements were carried out using the Physical Property Measurement System (PPMS), and the thermal conductivity was derived by fitting the experimental data of 3ω measurements to a numerical model.[S21]

mal conductivity of the nanowires through fitting of the experimental data. In the past, many theories have been used to calculate the effective thermal conductivity of such composite structures, viz. Maxwell's effective media theory,[S22,S23] multiple-scattering approach,[S24] method of long waves[S25] and longitudinal shearing-transverse conduction analogy.[S26]

In our case, we have carried-out a finite element modelling (FEM) simulation using COMSOL^{TM} software considering a hexagonal arrangement of nanowires with a defined porosity as per the characteristics of the sample under study to numerically determine the anisotropy. It is assumed that the effective thermal conductivity depends on the volume fraction of the individual material and not on the arrangement of nanowires. Considering this fact, simulations have been carried out for hexagonal arrangement of nanowires with a contact resistance of 5×10^{-8}m^2.K.W^{-1} between the nanowires and amorphous AAO. Since, the nanowires have been electro-deposited and growth is guided by the internal geometry of the template, it is assumed that the nanowires are in good-thermal contact throughout the

lengths. The impact on roughness on the thermal contact resistance between the nanowires and AAO have been neglected in the model as size effects are negligible for amorphous materials.

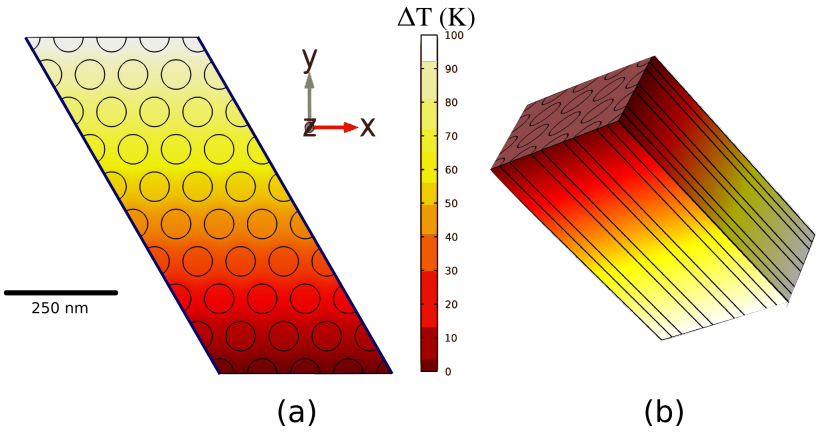

Figure S4: Temperature profile of (a) In-plane and (b) Cross-plane thermal transport. The colour suggests the rise in temperature in the state condition under the effect of effect of a temperature gradient.

The thermal conductivity of the empty nanoporous alumina templates have been derived by fitting the data of 3ω measurements performed from 80 K to 350 K using 2D heat conduction model.[S21] In figure S3, the variation of thermal conductivity and heat capacity of the empty nanoporous alumina templates are presented. In the FEM model, a constant temperature difference of 100 K is applied to the system in cross-plane and in-plane configurations. The temperature profile is calculated by solving the Fourier law in the steady state conditions, shown in figure S4, which is used to calculate the thermal conductivity of the composite film. The heat flux through the system varies with the thermal conductivity of the material. Yet, in the steady-state conditions, the temperature rise is independent of the materials that constitute the film and, at the same time, is dependent on the thermal conductivity of the whole composite film.

Taking into account the thermal conductivity of nanoporous alumina derived from 3ω measurement on empty AAO, an FEM model is developed for simulating the variation in anisotropy of the composite film with different thermal conductivity values of nanowires

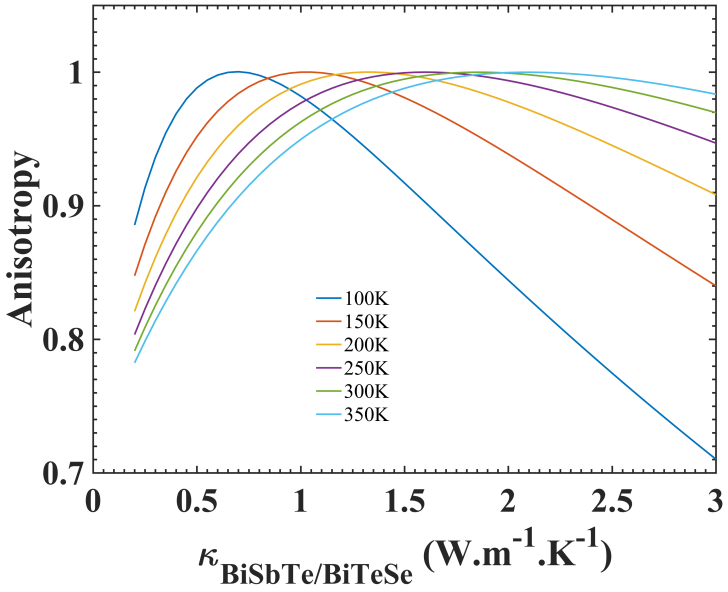

Figure S5: Numerical simulations for the estimation of thermal anisotropy using FEM for BiSbTe/BiTeSe NWs.

fed to the model at a particular temperature (as shown in figure S5). These variations in the anisotropy have been used to derive the thermal conductivity of the nanowires. In the data fitting process, the thermal conductivity was changed and based on the FEM model, the anisotropy was adjusted for the corresponding value of thermal conductivity.

Extraction of surface roughness

Multiple number of nanowires were studied in TEM and the micrographs are present in figure S7. The random surface roughness in the nanowires were studied and one of the example for $Bi_{1.45}Te_{2.85}Se_{0.7}$ nanowires is present in figure S11. The 1D power spectrum of the nanowires was calculated from the surface roughness profile of the nanowire after removing the background of the TEM image (as shown in figure S11c). The averaged power spectrum was then calculated by analysing and averaging various nanowires (figure present in the main text). The relation between the power spectrum and the wavevectors q was used to determine the correlation length. Similarly, the roughness and correlation length

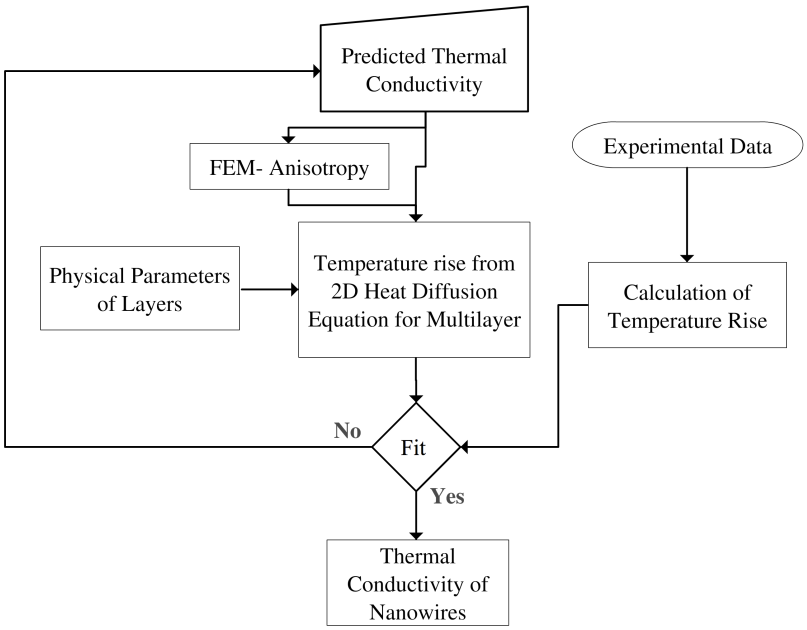

Figure S6: A flowchart for extracting the cross-plane thermal conductivity of nanowires from the experimental data.

calculations were carried out for all the nanowires.

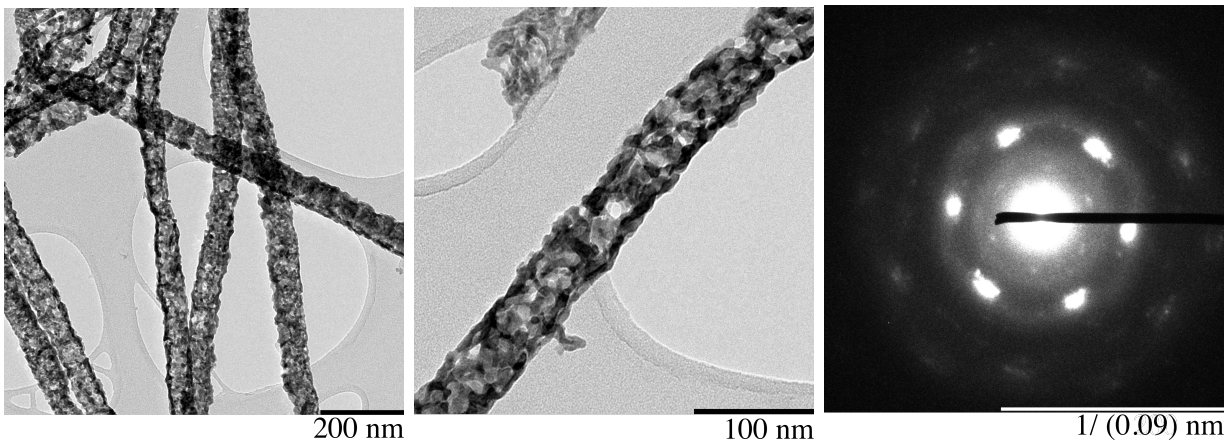

Figure S7: Structural analysis of $Bi_{1.45}Te_{2.85}Se_{0.7}$ nanowires by (a), (b) transmission electron microscopy, and (c) diffraction pattern of the nanowire.

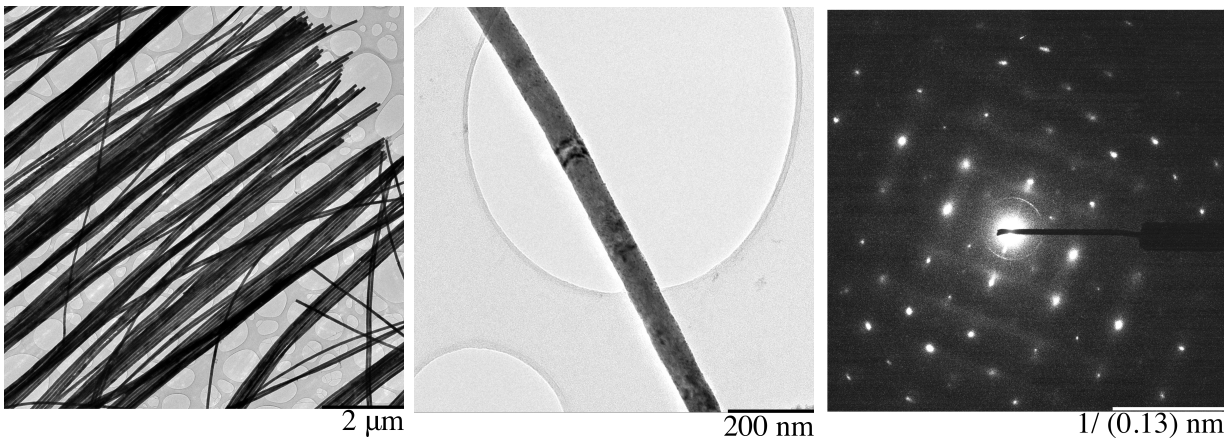

Figure S8: Structural analysis of $Bi_{1.55}Te_{2.9}Se_{0.55}$ nanowires by (a), (b) transmission electron microscopy, and (c) diffraction pattern of the nanowire.

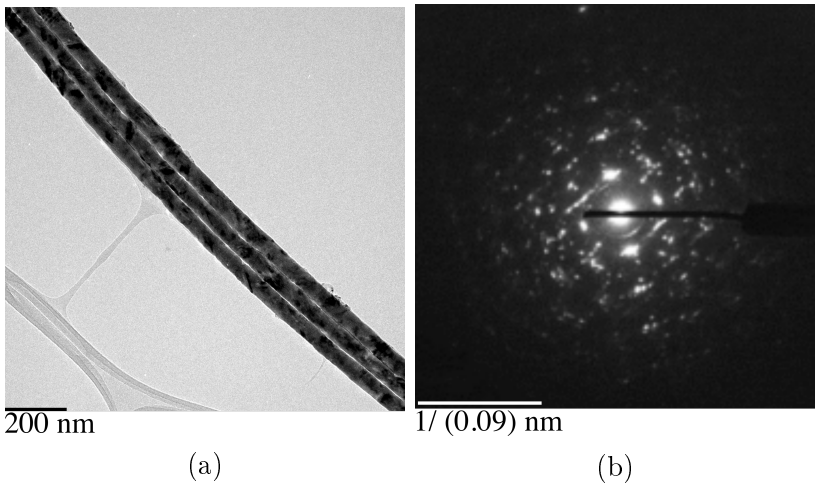

Figure S9: Structural analysis of $Bi_{0.4}Sb_{1.43}Te_{3.17}$ nanowires by (a), and (b) diffraction pattern of the nanowire.

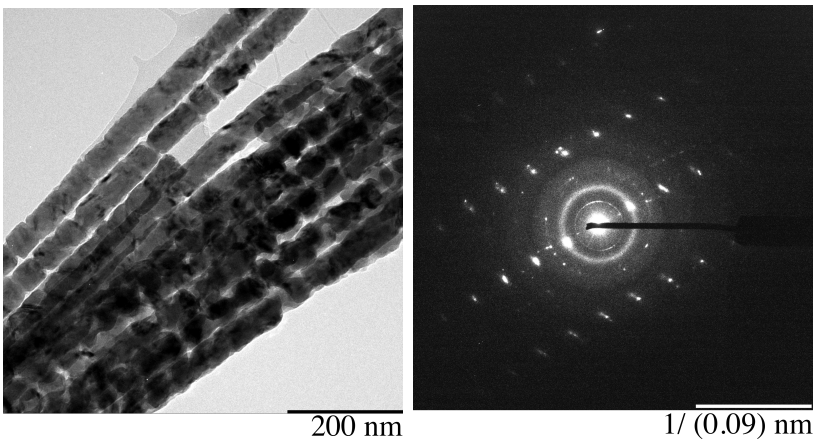

(a) (b)

Figure S10: Structural analysis of $Bi_{0.6}Sb_{1.85}Te_{2.55}$ nanowires by (a), and (b) diffraction pattern of the nanowire.

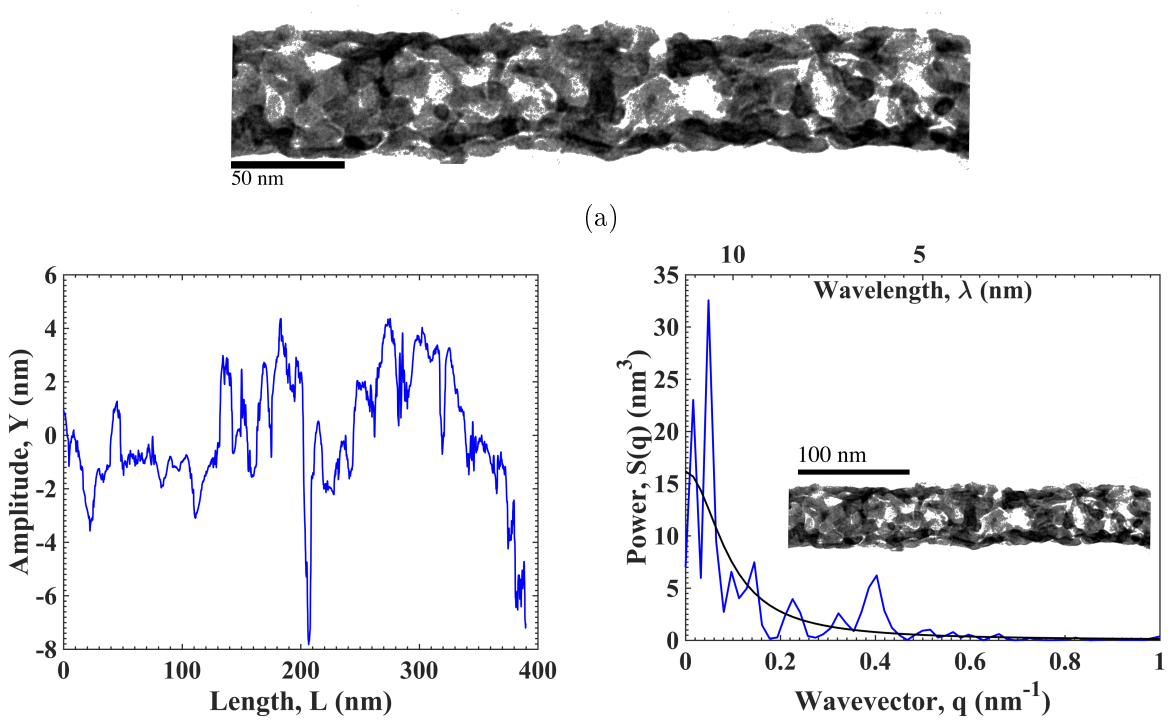

(a) (b) (c)

Figure S11: Roughness analysis for $Bi_{1.45}Te_{2.85}Se_{0.7}$ nanowires. (a) Nanowire image after background removal which was initially retrieved by TEM, (b) surface roughness profile of the nanowire around the mean value, (c) calculated power factor $S(q)$ by taking the Fourier transform of (b).

Determination of uncertainty in thermal conductivity

While determining the thermal conductivity through the 3ω method, primarily, two sources of error could arise. Firstly, from the experimental measurements of the temperature rise on the metal line coming from the setup and, secondly from the extraction of thermal conductivity from the 2D heat diffusion equation consisting of various physical parameters of the sample.

Relative error of the setup

The thermal conductivity of the sample is extracted by fitting the amplitude of temperature rise in the metal line (ΔT). There are uncertainties arising from the experimental setup and from the derivation of the temperature coefficient α.

From the relationship

$$\Delta T = \frac{2V_{3\omega}}{I(\mathrm{d}R/\mathrm{d}T)} \tag{S6}$$

we derive the uncertainty by deriving the total differential of (ΔT) :

$$\left\| \frac{\mathrm{d}(\Delta T)}{(\Delta T)} \right\| \equiv \frac{\Delta(\Delta T)}{(\Delta T)} = \sqrt{\left(\frac{\mathrm{d}V_{3\omega}}{V_{3\omega}}\right)^2 + \left(\frac{\mathrm{d}I}{I}\right)^2 + \left(\frac{\mathrm{d}(\mathrm{d}R/\mathrm{d}T)}{(\mathrm{d}R/\mathrm{d}T)}\right)^2} \tag{S7}$$

Note here that both uncertainties coming from the resistance and the slope of the resistance versus temperature are added together because they are correlated. The accuracy of both $V_{3\omega}$ and I are given by the specifications of the lock-in amplifier and the current source. For the lock-in amplifier (AMETEK 7124) the accuracy is $\pm 1\%$ of the full-scale sensitivity. The current source accuracy (home-made setup) is $\pm 0.05\% + 10\ \mu$A for the 20 mA range. The resistance is measured with (home-made TRMC2) an accuracy of $\pm 0.05\%$.

The uncertainty of the slope $(\mathrm{d}R/\mathrm{d}T)$ is extracted from the standard error of every coefficient given by the resulting fit of the resistance. The resistance R is fitted with a polynomial function :

$$R = \sum_{i=0}^{N} a_i T^i \tag{S8}$$

which derivative is given by

$$\frac{\mathrm{d}R}{\mathrm{d}T} = \sum_{i=0}^{N} i a_i T^{i-1} \tag{S9}$$

where T is the temperature, a_i the coefficients and N the order of the polynomial. The absolute error on $(\mathrm{d}R/\mathrm{d}T)$ is given by

$$\Delta(\mathrm{d}R/\mathrm{d}T) = \sqrt{\sum_{i=0}^{N} \left(i \Delta a_i T^{i-1}\right)^2} \tag{S10}$$

if we assume that the relative error on the temperature $\Delta T/T$ is small with respect to the relative error of the coefficients $\Delta a_i/a_i$. For example, if the resistance is well fitted with an order 2 polynomial :

$$R = a_0 + a_1 T + a_2 T^2 \tag{S11}$$

then

$$\mathrm{d}R/\mathrm{d}T = a_1 + 2a_2 T = A + B \tag{S12}$$

where we have defined $a_1 \equiv A$ and $2a_2 T \equiv B$. The relative error on B is

$$\frac{\Delta B}{B} = \sqrt{\left(\frac{\Delta a_2}{a_2}\right)^2 + \left(\frac{\Delta T}{T}\right)^2} \tag{S13}$$

hence

$$\Delta B = B\sqrt{\left(\frac{\Delta a_2}{a_2}\right)^2 + \left(\frac{\Delta T}{T}\right)^2} = B\left(\frac{\Delta a_2}{a_2}\right) = 2a_2 T\left(\frac{\Delta a_2}{a_2}\right) = 2T\Delta a_2 \tag{S14}$$

the error on $\mathrm{d}R/\mathrm{d}T$ is then

$$\Delta(\mathrm{d}R/\mathrm{d}T) = \sqrt{(\Delta A)^2 + (\Delta B)^2} = \sqrt{(\Delta a_1)^2 + (2T\Delta a_2)^2} \tag{S15}$$

which is equation (S10) for N=2. The assumption $\Delta T/T \ll \Delta a_i/a_i$ is true according to our experimental values. At 300 K with our PID setting we read $T = 300 \pm 0.003$ K which represents 10^{-3} % whereas $\Delta a_i/a_i$ is at least a few percent. We have access to the Δa_i values after doing a regression analysis. Generally, $\Delta(\mathrm{d}R/\mathrm{d}T)/(\mathrm{d}R/\mathrm{d}T) \approx 1\%$, which leads to $\Delta(\Delta T/T) \approx 1.8\%$. The uncertainty mentioned under the 'experimental' section define the percentage error in determination of the temperature rise plus the error from fitting the non-linear curve with the previously derived values of AAO (whose error is also considered).

Thermal Boundary Resistance

The temperature variation of thermal boundary resistance in between the metal line, the insulating alumina top layer and the substrate is experimentally determined through differential 3ω method using different thicknesses of the alumina films. The error mentioned in the 'TBR' section refers to the uncertainty arising in the value of the thermal conductivity when these measured TBR are changed during the fitting process between their extreme points ($1 \times 10^{-8} - 7 \times 10^{-8}$ W.m^2.K^{-1}).

Anisotropy

As the arrangement of the nanopores is nearly hexagonal, the porosity is observed through SEM images from the top side and back side of the AAO. The calculation of thermal conductivity are made while taking the average between the top and the bottom side. As a matter of fact, this porosity decreases along the length of the pores. If the considerations are made for the extreme porosities observed in the AAO template, the value of anisotropy changes and its effect on the thermal conductivity value as mentioned under the 'anisotropy' section. Other sources of error, which include the physical parameters like the specific heat and the thickness of the layer, were measured with high accuracy and were found to have a negligible impact on the final determined thermal conductivity.

Monte Carlo simulation of Bi_2Te_3 bulk and nanowire

The thermal conductivity of nanostructures like thin films and nanowires can be obtained by solving the Boltzmann Transport Equation (BTE) in the frame of the relaxation time approximation. This can be done using different numerical techniques, among them the Monte Carlo solution of the BTE has demonstrated its ability to model nano- and micro-structured semiconductors. In the present work, the techniques developed for the modelling of silicon nanowires[S27,S28] were used for Bi_2Te_3nanowire modelling.

With this MC technique the square nanowires (70 nm$\times$ 70 nm) with length of 1 μm are considered. A thermal gradient ΔT=4 K is set between the bottom and the top of the nanowire and film (bulk case) in order to derive the thermal conductivity from phonon heat flux calculation. The latter phonon transport property, is statistically derived from energy carriers displacement and scattering. Basically, with this technique phonons are described by energy quanta that are allow to drift and scatter through Normal, Umklapp and Impurity interactions. The main distinction between nanowire and thin film lies in the phonon scattering boundary condition set on the edge of the structure. For thin film phonons are specularly reflected and thus no thermal resistance is considered, while in nanowires phonon are diffusely reflected. This technique is extensively detailed in the above reference. Here, the main new input lies in the evaluation of phonon lifetime. They are derived from isotropic assumption of phonon dispersion along a and c axis of Bi_2Te_3, Gruneisen parameter and Debye temperature according to Morelli *et. al.*[S29]

As explained in the manuscript, further thermal conductivity reduction can be expected adding a supplementary lifetime for the phonon grain boundary scattering. In practice, depending on the grain size, the phonon mean free path can be decreased, especially at lower temperatures where only impurity and defect scattering dominate.

References

[S1] Masuda, H.; Fukuda, K. Ordered metal nanohole arrays made by a two-step replication of honeycomb structures of anodic alumina. *Science* **1995**, *268*, 1466–1468.

[S2] Bu, L.; Wang, W.; Wang, H. Electrodeposition of n-type Bi_2Te_3- ySe_y thermoelectric thin films on stainless steel and gold substrates. *Appl. Surf. Sci.* **2007**, *253*, 3360–3365.

[S3] Del Frari, D.; Diliberto, S.; Stein, N.; Boulanger, C.; Lecuire, J.-M. Comparative study of the electrochemical preparation of Bi_2Te_3, Sb_2Te_3, and $(Bi_xSb_(1-x)2)Te_3$ films. *Thin Solid Films* **2005**, *483*, 44–49.

[S4] Dresselhaus, M.; Heremans, J. Recent developments in low-dimensional thermoelectric materials. *Thermoelectric Handbook; Macro to Nano, Ed. by Rowe, CRC press, Boca Raton, FL* **2006**,

[S5] Goldsmid, H. Recent studies of bismuth telluride and its alloys. *J. Appl. Phys.* **1961**, *32*, 2198–2202.

[S6] Khedim, M. B.; Cagnon, L.; Serradeil, V.; Fournier, T.; Bourgault, D. Thermoelectric nanowires based on bismuth telluride. *Mater. Today:. Proc.* **2015**, *2*, 602–609.

[S7] Cahill, D. G.; Pohl, R. O. Thermal conductivity of amorphous solids above the plateau. *Phys. Rev. B* **1987**, *35*, 4067.

[S8] Cahill, D. G.; Fischer, H. E.; Klitsner, T.; Swartz, E.; Pohl, R. Thermal conductivity of thin films: measurements and understanding. *J. Vac. Sci. Technol. A* **1989**, *7*, 1259–1266.

[S9] Cahill, D. G. Thermal conductivity measurement from 30 to 750 K: the 3ω method. *Rev. Sci. Instrum.* **1990**, *61*, 802–808.

[S10] Lee, S.-M.; Cahill, D. G.; Venkatasubramanian, R. Thermal conductivity of Si–Ge superlattices. *Appl. Phys. lett.* **1997**, *70*, 2957–2959.

[S11] Borca-Tasciuc, T.; Kumar, A.; Chen, G. Data reduction in 3ω method for thin-film thermal conductivity determination. *Rev. Sci. Instrum.* **2001**, *72*, 2139–2147.

[S12] Borca-Tasciuc, D.-A.; Chen, G. Anisotropic thermal properties of nanochanneled alumina templates. *J. Appl. Phys.* **2005**, *97*, 084303.

[S13] Chen, G.; Zhou, S.; Yao, D.-Y.; Kim, C.; Zheng, X.; Liu, Z.; Wang, K. Heat conduction in alloy-based superlattices. *Thermoelectrics, 1998. Proceedings ICT 98. XVII International Conference on* **1998**, 202–205.

[S14] Dames, C.; Chen, G. $1\,\omega$, $2\,\omega$, and $3\,\omega$ methods for measurements of thermal properties. *Rev. Sci. Instrum.* **2005**, *76*, 124902.

[S15] Liu, Y.; Tainoff, D.; Boukhari, M.; Richard, J.; Barski, A.; Bayle-Guillemaud, P.; Hadji, E.; Bourgeois, O. Sensitive 3-omega measurements on epitaxial thermoelectric thin films. *IOP Conference Series: Materials Science and Engineering* **2014**, *68*, 012005.

[S16] Bourgeois, O.; Fournier, T.; Chaussy, J. Measurement of the thermal conductance of silicon nanowires at low temperature. *J. Appl. Phys.* **2007**, *101*, 016104.

[S17] Jaramillo-Fernandez, J.; Ordonez-Miranda, J.; Ollier, E.; Volz, S. Tunable thermal conductivity of thin films of polycrystalline AlN by structural inhomogeneity and interfacial oxidation. *Phys. Chem. Chem. Phys.* **2015**, *17*, 8125–8137.

[S18] Rosenthal, L. A. Thermal response of bridgewires used in electroexplosive devices. *Rev. Sci. Instrum.* **1961**, *32*, 1033–1036.

[S19] Holland, L. R.; Smith, R. C. Analysis of temperature fluctuations in ac heated filaments. *J. Appl. Phys.* **1966**, *37*, 4528–4536.

[S20] Birge, N. O.; Nagel, S. R. Wide-frequency specific heat spectrometer. *Rev. Sci. Instrum.* **1987**, *58*, 1464–1470.

[S21] Singhal, D.; Paterson, J.; Tainoff, D.; Richard, J.; Ben-Khedim, M.; Gentile, P.; Cagnon, L.; Bourgault, D.; Buttard, D.; Bourgeois, O. Measurement of anisotropic thermal conductivity of a dense forest of nanowires using the 3ω method. *Rev. Sci. Instrum.* **2018**, *89*, 084902.

[S22] Levin, M.; Miller, M. Maxwell a treatise on electricity and magnetism. *Uspekhi Fizicheskikh Nauk* **1981**, *135*, 425–440.

[S23] Hasselman, D.; Johnson, L. F. Effective thermal conductivity of composites with interfacial thermal barrier resistance. *J. Compos. Mater.* **1987**, *21*, 508–515.

[S24] Nan, C.-W.; Birringer, R.; Clarke, D. R.; Gleiter, H. Effective thermal conductivity of particulate composites with interfacial thermal resistance. *J. Appl. Phys.* **1997**, *81*, 6692–6699.

[S25] Behrens, E. Thermal conductivities of composite materials. *J. Compos. Mater.* **1968**, *2*, 2–17.

[S26] Hashin, Z. Analysis of composite materials—a survey. *J. Appl. Mech.* **1983**, *50*, 481–505.

[S27] Lacroix, D.; Joulain, K.; Terris, D.; Lemonnier, D. Monte Carlo simulation of phonon confinement in silicon nanostructures: Application to the determination of the thermal conductivity of silicon nanowires. *Appl. Phys. Lett.* **2006**, *89*, 103104.

[S28] Jean, V.; Fumeron, S.; Termentzidis, K.; Zianni, X.; Lacroix, D. Monte Carlo simulations of phonon transport in Si nanowires with constrictions. *Int. J. Heat Mass Transfer* **2015**, *86*, 648–655.

[S29] Morelli, D.; Heremans, J.; Slack, G. Estimation of the isotope effect on the lattice thermal conductivity of group IV and group III-V semiconductors. *Phys. Rev. B* **2002**, *66*, 195304.